Biomaterials Science

ROYAL SOCIETY OF CHEMISTRY

PAPER

View Article Online
View Journal

Check for updates

Cite this: DOI: 10.1039/d3bm00477e

Membrane interaction and selectivity of novel alternating cationic lipid-nanodisc assembling polymers†

Michelle D. Farrelly, [a] Jiali Zhai, [b] Alice Y. J. Tiong, [c] Leonie van 't Hag, [c] Heidi H. Yu,[d] Jian Li,[d] Lisandra L. Martin *[a] and San H. Thang *[a]

Synthetic polymer nanodiscs are self-assembled structures formed from amphipathic copolymers encapsulating membrane proteins and surrounding phospholipids into water soluble discs. These nanostructures have served as an analytical tool for the detergent free solubilisation and structural study of membrane proteins (MPs) in their native lipid environment. We established the polymer–lipid nanodisc forming ability of a novel class of amphipathic copolymer comprised of an alternating sequence of *N*-alkyl functionalised maleimide (AlkylM) of systematically varied hydrocarbon chain length, and cationic *N*-methyl-4-vinyl pyridinium iodide (MVP). Using a combination of physicochemical techniques, the solubilisation efficiency, size, structure and shape of DMPC lipid containing poly(MVP-*co*-AlkylM) nanodiscs were determined. Lipid solubilisation increased with AlkylM hydrocarbon chain length from methyl (MM), ethyl (EtM), *n*-propyl (PM), iso-butyl (IBM) through to *n*-butyl (BM) maleimide bearing polymers. More hydrophobic derivatives formed smaller sized nanodiscs and lipid ordering within poly(MVP-*co*-AlkylM) nanodiscs was affected by nanodisc size. In dye-release assays, shorter *N*-alkyl substituted polymers, particularly poly(MVP-*co*-EtM), exhibited low activities against eukaryotic mimetic POPC membrane and increased their liposome disruption as POPC : POPG membrane mixtures increased in their anionic POPG component, resembling the charge profile of bacterial membranes. These trends in membrane selectivity were transferred towards native cell systems in which gram-positive *Staphylococcus aureus* and gram-negative *Acenobacter baumannii* bacterial strains were relatively susceptible to disruption by hydrophobic *n*-butyl- and *n*-propyl-poly(MVP-*co*-AlkylM) derivatives compared to human red blood cells (HRBCs), with a more pronounced selectivity resulting from poly(MVP-*co*-PM). Such selective membrane interaction by less hydrophobic polymers provides a framework for polymer design towards applications including selective membrane component solubilisation, biosensing and antimicrobial development.

Received 18th March 2023,
Accepted 8th July 2023

DOI: 10.1039/d3bm00477e

rsc.li/biomaterials-science

Published on 18 July 2023. Downloaded by University of Alberta on 8/1/2023 12:02:35 PM.

Introduction

Membrane proteins (MPs) are embedded within or associated with the phospholipid bilayer which encases and compartmentalises biological cells.[1,2] Although membrane proteins have significant consequence in biological processes making them predominant targets for drugs, their structures are underrepresented in the protein database due to inherent difficulties involved in their biophysical characterisation whilst retaining their structural integrity.[3–5] Recent years have seen rapid expansion in cryo-EM resolved MP structures[6–8] as a result of advances in the field. Thus, the question of how to conformationally stabilise native structures of MPs is all the more important.[9] Styrene maleic acid (SMA) polymer nanodiscs have demonstrated a broad applicability in solubilising a vast range of MPs along with their surrounding lipid bilayer annulus without the introduction of potentially denaturing detergents in the process.[10–12] During the formation of styrene maleic acid lipid particles (SMALPs), the active polymer directly extracts membrane proteins either from native cellular membranes or from an intermediary reconstituted synthetic membrane system to yield self-assembled nanodisc structures of a general 10–12 nm diameter.[13,14] SMALPs have shown no preferential lipid solubilisation across various binary lipid compo-

[a]School of Chemistry, Monash University Clayton, VIC 3800, Australia. E-mail: lisa.martin@monash.edu, san.thang@monash.edu
[b]School of Science, STEM College, RMIT University Melbourne, VIC 3000, Australia
[c]Department of Chemical and Biological Engineering, Monash University, Clayton, VIC 3800, Australia
[d]Infection Program and Department of Microbiology, Biomedicine Discovery Institute, Monash University Clayton, VIC 3800, Australia

† Electronic supplementary information (ESI) available. See DOI: https://doi.org/10.1039/d3bm00477e

Published on 18 July 2023. Downloaded by University of Alberta on 8/1/2023 12:02:35 PM.

sitions,[15] a feature which allows for the general applicability of SMA in the reconstitution of a wide range of integral MPs for structural and functional characterisation.[16–18] It is notable that overall SMALP solubilisation efficiency is affected by membrane lipid composition. For instance, the higher fractions of cardiolipin (CL) and phosphatidylethanolamine (PE) lipids are found in membrane compositions that do not readily form SMALPs.[19] Research into novel polymer nanodisc materials which are selective towards specific membrane lipid compositions, such as bacterial membranes in preference to mammalian membranes, holds potential for a myriad of applications. These include antimicrobial surfaces, drug discovery, biosensing, targeted drug delivery and selective extraction and separation of membrane proteins enriched in specific phospholipid combinations.

Bacterial membranes are composed of a higher proportion of negative phospholipids compared to mammalian and eukaryotic membranes which primarily express zwitterionic phospholipids.[20] These more negatively charged membranes can be vulnerable to disruption by cationic compounds and polymers, a principle schematised by Fig. 1A. For instance, polymers containing cationic moieties such as 4-vinyl methylpyridinium iodide have shown selective antimicrobial activity within nanostructured spherical and rod-like polymer brushes.[21] If amphipathic nanodisc polymer materials can be constructed with controlled sequences exhibiting a balance of cationic and hydrophobic units, a principle often used to design membrane active antimicrobials (MAAs),[21,22] selective membrane disruption and solubilisation is expected to be realised. We have explored the nanodisc assembly and membrane selectivity of a novel RAFT[23–25] synthesised class of alternating cationic polymers comprised of hydrophobic alkyl (specifically methyl, ethyl, *n*-propyl, *n*-butyl and iso-butyl) functionalised maleimide units and hydrophilic *N*-methyl-4-vinyl pyridinium iodide also called (poly(MVP-*co*-AlkylM)s) shown in Fig. 1B. Membrane selectivity was measured by the polymer disruption of model membrane liposome systems comprised of systematically varied phospholipid composition and surface charge. Potential antimicrobial implications of the discovered selective polymer properties were explored to determine if patterns in selectivity towards synthetic membranes can be translated to whole cells. Complimentary biophysical techniques were employed including phosphorus nuclear magnetic resonance (^{31}P NMR), dynamic light scattering (DLS), transmission electron microscopy (TEM) and small angle X-ray scattering (SAXS) to examine the solubilisation efficiency and dimensions of empty polymer–lipid nanodisc assemblies. Laurdan fluorescence and differential scanning calorimetry (DSC) aided exploration into the physical properties of lipids within nanodiscs of variable size, before dye-release and antimicrobial assays were used to study the selectivity of membrane disruption and the possibility of implementations related to bacterial growth inhibition.

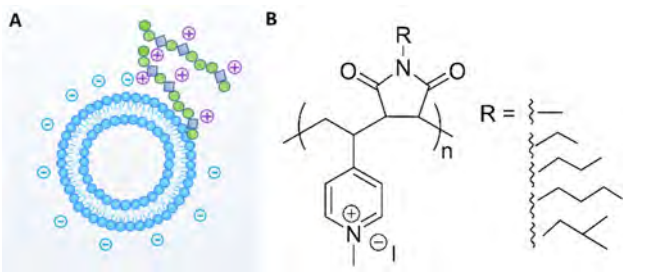

Fig. 1 (A) Illustration of electrostatic membrane interactions between bacterial mimetic liposomes and amphipathic copolymers with cationic moieties. (B) Chemistry of cationic poly(*N*-methyl-4-vinyl pyridinium iodide-*co*-*N*-alkyl-maleimide) alternating copolymers (alkyl = methyl, ethyl, *n*-propyl, iso-butyl and *n*-butyl).

Experimental section

Materials

4-Vinyl pyridine (≥95%, Sigma-Aldrich) was purified by passing through a basic alumina column. Azobisisobutyronitrile (AIBN) initiator was purchased from Wako Chemical. Iodomethane (99%, ACROS Organics™), *n*-butylamine (99.5%, Sigma-Aldrich), iso-butylamine (99%, Sigma-Aldrich), sodium acetate (≥99.0, Merck), acetic anhydride (≥98.0, Merck), *N*-methyl maleimide (97%, TCI), *N*-ethyl maleimide (≥98, Sigma-Aldrich) and *N*-*n*-propyl maleimide (95%, Sigma-Aldrich) were used as received. 4-Cyano-4-[(dodecylsulfanylthiocarbonyl)sulfanyl]pentanoic acid (≥99%, $C_{12}H_{25}$RAFT) and 4-((((2-carboxyethyl)thio)carbonothioyl)thio)-4-cyanopentanoic acid (95%) were purchased from Boron Molecular. Other solvents used were analytical or high-performance liquid chromatography (HPLC) grade.

50 mM TRIS-HCl buffer constituted Trizma® base (≥99.9%, Sigma) and 150 mM NaCl adjusted to the pH of 8.00 ± 0.02 by dropwise addition of ~0.1 M HCl. 10× (100 mM) HEPES buffer was comprised of 4-(2-hydroxyethyl)-1-piperazineethanesulfonic acid (HEPES, 99% Sigma-Aldrich), 1.35 M potassium chloride (KCl, 99.5%, Merck) and 10 mM magnesium chloride hexahydrate ($MgCl_2{\cdot}6H_2O$, Sigma-Aldrich) adjusted to the pH of 7.40 ± 0.02 by dropwise addition of ~0.1 M NaOH. 1× (10 mM) HEPES was prepared by a 10-fold dilution of 10× HEPES prior to dye-release assay experiments. High salt phosphate-buffered saline (HS PBS) was prepared with potassium phosphate monobasic (99% KH_2PO_4, Sigma), potassium phosphate dibasic (98% K_2HPO_4, Sigma-Aldrich) and sodium chloride (NaCl, Sigma) before adjusting the pH to 7.40 ± 0.02 with either ~0.1 M HCl or ~0.1 M NaOH. Phospholipids 1,2-dimyristoyl-*sn-glycero*-3-phosphocholine (DMPC) and 1-palmitoyl-2-oleoyl-*sn-glycero*-3-phosphoethanolamine (POPE) were purchased from Avanti® Polar Lipids. 1-Palmitoyl-2-oleoyl-*sn-glycero*-3-phosphocholine (POPC) and 1-palmitoyl-2-oleoyl-*sn-glycero*-3-phospho-(1′-*rac*-glycerol) (sodium salt) (POPG) were purchased from Cayman Chemical and cardiolipin sodium salt (sourced from bovine heart) was from Sigma-Aldrich. The fluorescent dye 5(6)-carboxyfluorescein (CF, 95%, Sigma-Aldrich) was used to detect membrane disruption, and Triton

This journal is © The Royal Society of Chemistry 2023

Published on 18 July 2023. Downloaded by University of Alberta on 8/1/2023 12:02:35 PM.

X-100 (Sigma-Aldrich) was used to determine complete membrane disruption.

Diblock styrene maleic acid (SMA, D10) copolymer synthesis

Diblock R-(Sty)-*b*-(Sty-*alt*-MA)-Z copolymer D10, used as an SMA benchmark for comparison in SAXS analysis, utilised the hydrophilic 4-((((2-carboxyethyl)thio)carbonothioyl)thio)-4-cyanopentanoic acid (COOH–C_2H_4RAFT) RAFT agent with the target monomer ratio 2 : 1 Sty : MAnh and target molecular weight of 6130. The *a*-block (poly(Sty)) reaction involved a [Sty] : [COOH–C_2H_4RAFT] : [AIBN] ratio of 20 : 1 : 0.1 and the subsequent alternating *b*-block used a [polymer] : [Sty] : [MAnh] : [AIBN] reaction mixture of 1 : 20 : 20 : 0.1. Dioxane solvent was used for both polymerisation reactions. Reaction mixtures were transferred to a Young vessel and degassed by three freeze–pump–thaw cycles before placing the sealed vessel in an oil bath at 70 °C for 24 hours. The viscous solution obtained was diluted in a minimal volume of dioxane and precipitated in isopropanol before recovery by vacuum filtration. The redissolution and precipitation procedure was repeated, and the powdered copolymer was vacuum oven dried.

Hydrolysis was then undertaken to ring-open the SMAnh copolymer into SMA in an overall 2 : 1 THF : water solution. Triethylamine (TEA) base was added in a molar ratio of 5.2 × MAnh unit per polymer. This procedure initially dissolved the polymer which was then stirred at 100 °C for 2 h. Hydrolysed polymer was precipitated using 1 M HCl, decanted and then redissolved in minimal ethanol, the precipitation and decantation was repeated once before fumehood drying. Hydrolysis of poly(styrene-*co*-maleic anhydride) to poly(styrene-*co*-maleic acid) using TEA was confirmed using ATR-IR. Diblock SMA was then separated from residual HCl and low molecular weight products by dissolution in Tris 20 mM (pH = 8.0) and dialysis against 1 L of the same buffer for 24 h with one buffer change, NaOH was added to the polymer solution to attain a pH of 8 before freeze-drying at −80 °C and refrigerated at 4 °C until ready for use. Number-average molar mass (M_n = 4500), weight-average molar mass (M_w = 5100) and dispersity ($Đ$ = M_w/M_n = 1.13) of SMA D10 was obtained from GPC of the hydrolysed product and the M_n and Sty : MA ratio were extrapolated from the ^{1}H NMR spectrum of the purified SMAnh product (M_n = 5000, Sty : MA = 1.7 : 1).

RAFT cationic poly(*N*-methyl-4-vinyl pyridinium iodide-*co*-*N*-alkyl-maleimide) synthesis

The monomers 4-vinyl pyridine (after running through a basic alumina column) and *N*-(alkyl)-maleimide comprising either *N*-methyl, *N*-ethyl, *N*-*n*-propyl, *N*-iso-butyl or *N*-*n*-butyl maleimide, were mixed with $C_{12}H_{25}$RAFT agent according to the following molar ratios: 42 : 50 : 1 : 0.1 [4VP] : [EtM or PM or IBM or BM] : [RAFT] : [AIBN] and 50 : 60 : 1 : 0.1 [4VP] : [MM] : [RAFT] : [AIBN] for the methyl–maleimide derivative. Reagents were transferred to a Young vessel with dioxane and a few drops of DMF to dissolve all components. The reaction mixture was degassed by three freeze–pump–thaw cycles before placing the sealed vessel in a 70 °C oil bath for 24 hours. The viscous solution obtained was diluted in a minimal volume of dioxane/DMF and precipitated in diethyl ether before recovery by vacuum filtration. The redissolution and precipitation procedure was repeated once and resulting powdered copolymer was dried under vacuum. Number-average molar mass (M_n), weight-average molar mass (M_w) and dispersity ($Đ$ = M_w/M_n) of copolymers were obtained from GPC. M_n was separately derived from ^{1}H NMR by combining the monomer conversion determined from crude ^{1}H NMR spectral integration and the monomer ratio given by pure ^{1}H NMR spectral peak integration. Percentage 4-vinyl pyridine monomer conversion and monomer ratios were determined by crude and pure ^{1}H NMR spectra in either d_6-acetone or d_6-DMSO depending on solubility. Poly(*N*-methyl-4-vinyl pyridinium iodide-*co*-*N*-methylmaleimide) (4VP-*co*-MM), poly(*N*-methyl-4-vinyl pyridinium iodide-*co*-*N*-ethylmaleimide) (4VP-*co*-EtM), poly(*N*-methyl-4-vinyl pyridinium iodide-*co*-*N*-*n*-propylmaleimide) (4VP-*co*-PM), poly(*N*-methyl-4-vinyl pyridinium iodide-*co*-*N*-iso-butylmaleimide) (4VP-*co*-IBM) and poly (*N*-methyl-4-vinyl pyridinium iodide-*co*-*N*-*n*-butylmaleimide) (4VP-*co*-BM) exhibited 62%, 76%, 74%, 69.9% and 61% 4-VP conversions, respectively.

Excess Iodomethane (in a molar ratio of 3 × 4-VP units per polymer) was added to each of the 4-vinyl pyridine-*co*-*N*-alkyl-maleimide polymers in DMF to quaternise the 4-vinyl pyridine monomer unit into *N*-methyl-4-vinyl pyridinium iodide. The mixture was reacted for 24 h at 45 °C, followed by precipitation in diethyl either and recovery by vacuum filtration. Resulting viscous precipitate was diluted with DMF again and dried under N_2 flow for several days. Worked-up polymers were then dialysed against Tris 20 mM (pH = 8.0) with a 2000–3500 Da MW cut-off dialysis membrane, the buffer was exchanged for distilled water after 6 h and was allowed to dialyse for a further 18 h. Polymer solutions were freeze-dried at −80 °C and then stored in a 4 °C fridge until ready for use.

Gel permeation chromatography (GPC)

GPC was performed with a system comprising a Shimadzu LC-20AT pump, Shimadzu RID-20A refractive index detector and SPD-20A UV-Visible detector. The GPC is equipped with a guard column (WAT054415) and 3 Waters GPC columns (WAT044238, WAT044226, WAT044235, 300 mm × 7.8 mm). The eluent was filtered dimethylformamide (DMF) containing 0.01 M lithium bromide (LiBr) at 40 °C (flow rate: 1 mL min^{-1}). Number average (M_n) and weight average (M_w) molecular weights were evaluated using Shimadzu software. A calibration curve was obtained from poly(methyl methacrylate) (PMMA) standards (Agilent) ranging from 960 to 1 568 000 g mol^{-1}. A third order polynomial was used to fit the log M_n *vs.* retention time calibration curve. Samples were prefiltered in DMF solvent using a 0.2 μm filter.

Lipid preparation and large unilamellar liposome (LUV) extrusion

Lipid stock solutions of DMPC were prepared by adding 100 μL aliquots of 50 mM DMPC dissolved in chloroform to

Published on 18 July 2023. Downloaded by University of Alberta on 8/1/2023 12:02:35 PM.

individual glass test tubes. Lipid mixtures (5 mM net lipid) of POPC, POPC : POPG (4 : 1), POPC : POPG (1 : 1) and POPE : POPG : cardiolipin (CL) (15 : 4 : 1) molar ratios for dye-release assays as well as DMPC : Laurdan (100 : 1) and POPC : POPG (1 : 1) (45.5 and 50 mM net solute component, respectively) were dispensed into test tubes as 100 μL aliquots. Mixtures were made up by combining individual lipid stock solutions (with POPC, POPE, CL and Laurdan each dissolved in chloroform and POPG dissolved in 2 : 1 chloroform : methanol (v/v)) in the designated ratios. Lipid mixtures were initially dried by rotating test tubes under a gentle stream of nitrogen, then desiccated under vacuum overnight and stored at −20 °C. Before lipid extrusion, frozen lipid mixtures were hydrated with 0.25–1 mL of the specified buffer, vortexed shortly, incubated at 37 °C for at least 30 minutes and vortexed for a further 2–5 minutes. Each hydrated lipid mixture was extruded through a polycarbonate membrane of 0.1 μm pore size or 0.2 μm pore size to form large unilamellar vesicles (LUVs) using a mini extruder apparatus (Avanti® Polar Lipids, Inc.) on a 40 °C heating block. Where necessary, LUVs were further diluted with buffer to meet the target lipid concentration.

Phosphorus nuclear magnetic resonance (^{31}P NMR)

Stock solutions of extruded 5 mM DMPC, POPC or POPC : POPG (1 : 1) in the form of 0.1 μm diameter LUVs and 2.5 mM polymer in deuterated buffer (50 mM Tris, 150 mM NaCl, 10% D_2O, pH 8.00 ± 0.02) were used to prepare samples containing 3.6 mM lipid and 0–0.71 mM polymer samples (in proportion to the specified lipid : ratio). After mixing, all samples were incubated at 26 °C for at least 24 h. Measurements were performed at 25 °C on a Bruker Avance III spectrometer operated at a ^{31}P resonance frequency of 162 MHz using a 5 mm triple resonance observe probe. 256 transients were acquired with an inverse-gated ^{1}H decoupling sequence (zgig30) using an acquisition time of 2.05 s, a sweep width of 64 103 Hz, and a relaxation delay of 6 s. A capillary containing 85% H_3PO_4 diluted in 1000-fold D_2O was used to provide lock and chemical shift referencing (δ = 0 ppm). ^{31}P NMR spectra were multiplied by an exponential function with a line-broadening factor of 1.0 Hz before Fourier transformation.

Zeta potential

Mean zeta potential for each polymer was determined from three replicate measurements of 0.625 mM polymer solution in Milli-Q® water. Experiments were performed at 25 °C on a Litesizer™ 500 particle analyser by Anton Parr with 50 runs per measurement in an Omega cuvette. The accompanying Kalliope software was used to compute zeta potential from the electrophoretic mobility using the Smoluchowski equation.

Dynamic light scattering (DLS)

To 1 mL of 1.25 mM lipid LUV (0.2 μm diameter) solution made up in the relevant buffer system (TRIS-HCl or 1× HEPES), 2.5 mM polymer solutions in buffer were added in either 50 μL or 100 μL aliquots to prepare solutions of 0.1 : 1 and 0.2 : 1 polymer : lipid ratios, respectively. For dye-release assays, dynamic light scattering (DLS) was conducted on dye-filled LUVs (<0.125 mM lipid) within a day of preparation. After at least 24 h of incubation, DLS experiments were performed at 25 °C on a Zetasizer Nano ZS (Malvern Instruments, Worcestershire, United Kingdom). Nanodisc samples were measured 3 consecutive times with 15 runs per measurement. Size-intensity distribution, size-volume distribution, PDI and Z-average size measurements were generated using ZETASIZER software version 7.13 and analysed using multiple narrow distribution. Where the Zetasizer Nano ZS was unavailable, DLS experiments were instead performed at 25 °C on a Litesizer™ 500 particle analyser by Anton Parr with 30 runs per measurement at a 175° backscatter angle. For the latter, size-intensity distribution, size-volume distribution, % PDI and hydrodynamic diameter measurements were generated using accompanying Kalliope software. Particle size determinations for Laurdan fluorescence and differential scanning calorimetry utilised the size-intensity distribution of smallest diameter peak (peak # 1).

Transmission electron microscopy (TEM)

A 1.25 mM buffered solution of DMPC 0.2 μm diameter LUVs was combined with aliquots from a 1.25 mM polymer solution in the specified polymer : lipid molar ratio. After at least 24 h incubation samples were diluted by a factor of 10–25 before coating TEM grids with sample. Copper grids (formvar/carbon coated, 400 mesh) were plasma glow-discharged for 20 seconds to create a hydrophilic surface after which the grids were contacted with a drop of the selected nanodisc mixture. After blotting to remove excess sample dispersion followed by a 10 seconds rinse with distilled water to remove excess salts from the buffer (for DMPC containing nanodisc samples only), the grids were negatively stained by contacting with a drop of uranyl acetate solution (0.5% w/v) for 1 minute and the grid was dried using a gentle nitrogen blow. Imaging was performed using a FEI Tecnai G2 T20 TWIN TEM instrument equipped with Orius SCD200D wide-angle CCD camera operating at 200 kV. Particle size histograms were constructed using imageJ analysis of TEM images by measuring at least 100 particles across two different axes. Histograms were fitted with a Gaussian distribution to determine the mean particle diameter.

Laurdan fluorescence

DMPC LUVs (0.1 μm diameter) were prepared as in the previously stated protocol with the additional incorporation of the Laurdan (*N*,*N*-dimethyl-6-dodecanoyl-2-naphthylamine) fluorescent probe into the lipid stock solutions in a 1 : 100 Laurdan to DMPC ratio. Lipid stock solutions were made up in chloroform, dried under a gentle N_2 stream, rehydrated to 4.5 mM DMPC with 10 mM HEPES, 135 mM KCl and 1 mM $MgCl_2$ (1× HEPES buffer, pH = 7.4 ± 0.02) and extruded through 0.1 μm pore-size polycarbonate membranes. Extruded liposomes were combined with polymer stock solutions in a

 This journal is © The Royal Society of Chemistry 2023

Published on 18 July 2023. Downloaded by University of Alberta on 8/1/2023 12:02:35 PM.

0.2 : 1 polymer : lipid molar ratio before 24 h incubation at 26 °C, followed by ultracentrifugation (100 000 *g*, 90 min, 4 °C) to pellet out unreacted liposomes or aggregates and buffer dilution to ultimately yield polymer/lipid samples containing ~32 μM DMPC overall.

Fluorescence emission spectra were obtained with a Cary Eclipse fluorescence spectrometer (Agilent) equipped with temperature control. Triplicate fluorescence spectra were acquired between 10–45 °C or 10–50 °C in 5 °C increments with scans across the 400 to 550 nm range. The excitation wavelength was set to 336 nm, excitation and emission bandpass were set to 10 nm and 5 nm, respectively and the temperature equilibration time was at least 15–20 min with manual monitoring to ensure spectral stability between runs. Averaged data were processed with initial buffer and baseline subtractions before generalized polarisation (GP) was calculated for each measurement according to the eqn (1) to construct GP *vs.* temperature plots for each sample condition. I_{435} and I_{500} refer to the emission intensity recorded at 435 nm and 500 nm, respectively.

$$\mathrm{GP} = (I_{435} - I_{500})/(I_{435} + I_{500}) \quad (1)$$

Differential scanning calorimetry (DSC)

The melting temperatures were measured using nano-differential scanning calorimetry (NanoDSC 602000, TA Instruments, USA), which utilises a platinum capillary cell that provides the sensitivity required to measure nanoparticles. As a lipid only control, 7.14 mM DMPC LUVs (0.1 μm diameter) were prepared in high salt phosphate-buffered saline (HS PBS) (pH = 7.4 ± 0.02) and poly(MVP-*co*-BM) nanodisc solutions comprised of 0.1 : 1 and 0 : 2 : 1 polymer : DMPC molar ratios also containing 7.14 mM DMPC, were made up in the same buffer prior to 24 h incubation at 26 °C. Nanodisc samples were ultracentrifuged (100 000*g*, 90 min, 4 °C) to pellet out unreacted liposomes or aggregates before degassing at 450 mmHg with a Vacuum Degassing System (TA instruments, USA), stirring at 100 rpm for 5 minutes to ensure the elimination of gas bubbles. Samples (750 μL) were loaded into the sample cell and HS PBS reference buffer (750 μL) into the reference cell. The solution was measured at 1 °C per minute from 10 °C to 50 °C and then back to 10 °C at 3 atm pressure. Between each sample measurement, NanoDSC cells were flushed with 150 mL of 99.9% ethanol, 100 mL of 1% (w/v) SDS, and 4 L of Milli-Q® water. Both NanoDSC cells were then soaked in 1 mg mL^{-1} of pepsin in 0.1 M acetic acid and 0.5 M NaCl for 3 hours at 30 °C before being flushed with 4 L of Milli-Q® water. The sample data was first aligned with buffer data using the Heating Rate at 40–55 °C followed by buffer subtraction. Phase transition temperatures were reported as the temperature (°C) at the maximum heat rate for each sample.

Small angle X-ray scattering (SAXS)

Polymer solutions (2.5 mM) were prepared in TRIS-HCl buffer (50 mM Tris, 150 mM NaCl, pH 8.00 ± 0.02). Polymers (diblock SMA D10 and MVP-*co*-BM) were each added to extruded 10 mM DMPC LUVs (with 0.2 μm pore membranes) in a 0.2 : 1 polymer : lipid ratio. Polymer/lipid samples and polymer only controls were incubated in a 26 °C water bath for 24 h, followed by ultracentrifugation (100 000 *g*, 90 min, 4 °C) to pellet out unreacted liposomes or aggregates. DLS was employed to verify sample quality regarding the degree of homogeneity and size distribution.

SAXS experiments were performed at the SAXS/WAXS beamline at the Australian Synchrotron, ANSTO, Melbourne, Australia. The SAXS data were recorded on a Pilatus2 1-M detector with the X-ray wavelength λ = 1.033 Å (12.0 keV) and a typical flux of around 10^{13} photons per s. The recorded two-dimensional X-ray diffraction images were integrated into one dimensional plots of scattering intensity (I) *versus* scattering vector ($q = 4\pi \sin(\theta)/\lambda$), where θ is the scattering angle and λ is the wavelength. The sample to detector distance was chosen as 1.6 m which provided a q-range of 0.075 to 0.7 $Å^{-1}$, however the q range of 0.075 to 0.3 $Å^{-1}$ was selected to remove scattering from the plastic plate above 0.4 $Å^{-1}$. Samples were loaded into a 96-well plate (Corning 96-Well Multiwell Plates), which was sealed using Corning Microplate Sealing Tape and run using the transmission SAXS set-up. Each well was scanned in two positions (with data from the first scan used in further analysis) with an exposure time of 1 second and three consecutive patterns were acquire for each position.[26] Scatterbrain 2.82 was used for SAXS data reduction, and Primus within the ATSAS software package was used for SAXS data analysis, with Guinier analysis used to obtain the radius of gyration (R_g) and indirect Fourier transform (IFT) to calculate the pair-distance distribution (P(r)) function and the maximum diameter (D_{max}).

Dye release assays

To prepare dye-filled liposomes, a 50 mM solution of 5(6)-carboxyfluorescein (CF) was made up in 10% 1 M sodium hydroxide and 90% 1× HEPES buffer (final pH = 6.1 ± 0.1). The resulting solution was vortexed for 30 seconds and centrifuged for a further 10 minutes to remove residual insoluble dye material. Preprepared dried lipid mixtures (POPC, POPC : POPG (4 : 1), POPC : POPG (1 : 1) and POPE : POPG : CL (15 : 4 : 1)) were rehydrated with (1 mL) supernatant dye solution to obtain 0.5 mM lipid within dye-saturated buffer dispersant before liposome extrusion was performed with 0.1 μm polycarbonate membranes using the previously described protocol. Extruded dye-loaded liposomes (0.5 mL) were separated from their surrounding dye solution using a PD-10 desalting column (GE Health Care Life Sciences, USA) loaded with Sephadex TM G-25 and equilibrated with 1× HEPES buffer. 2 mL of purified dye-loaded liposomes were collected from the column.

For membrane disruption studies, black polystyrene 96-well microplates from Greiner Bio-One (Germany) were used and dye release from the CF-loaded liposomes was detected using a CLARIOstar plate reader (BMG Labtech, Germany) with excitation and emission wavelengths of 485–10 and 535–10 nm, respectively. Triplicate experiments were performed at 25 °C with three seconds of double orbital shaking at 300 rpm prior

Published on 18 July 2023. Downloaded by University of Alberta on 8/1/2023 12:02:35 PM.

to measurement. Measurements were conducted for 45 cycles (cycle time = 106 seconds). Initially, 0% dye release baselines were recorded for 8 cycles measuring a 100 μL (diluted 10-fold in 1× HEPES buffer) liposome fraction in each well. 50 μL of polymer stock solution of variable concentration was then added to the system to attain the specified overall polymer concentration (ranging from 0.0067–0.0670 μM) demonstrating the full the range of membrane activity for each respective polymer. Measurements resumed for 27 cycles to monitor the % dye-release achieved by the polymer before 10 μL of 1% Triton X-100 was pipetted into each well to lyse any remaining dye-filled liposomes and fluorescence was measured for another 9 cycles. Concordant results were averaged, then plotted using GraphPad PRISM 9. Percentage dye-release *vs.* time plots were normalised by assigning 0% to the initial liposome baseline measurements and 100% to the final measurements after Triton X-100 addition. Percentage dye-release achieved by each polymer was calculated using the final baseline measurement (cycle 8) to denote 0% dye-release, the final measurement (at cycle 32) prior to the Triton X-100 addition to give the maximal percentage dye release, for which the maximum value across the measured concentration range was used, and the final measurements post Triton X-100 addition indicated 100% disruption.

Disk diffusion assays

Bacterial colonies (*Staphylococcus aureus* ATCC 29213 and *Acinetobacter baumannii* ATCC 17978) were swabbed from nutrient agar and resuspended in 0.9% w/v saline (McFarland = 0.5, *i.e.*, 1.5×10^8 CFU mL^{-1}). Nutrient agar plates were inoculated with bacterial cultures using a sterile swab.[27] Sterile discs with 10 μg colistin (Oxoid™) as a positive control, Milli-Q® water as a negative control and poly(MVP-*co*-AlkylM) cationic polymer derivatives (comprising methyl, ethyl, *n*-propyl or *n*-butyl maleimide substituents) with 5 mg or 2.5 mg polymer per disc, were placed onto agar plates which were incubated at 37 °C for 20 h. Relative antimicrobial activity as indicated by the measured zone of inhibition (ZOI) was determined after the set incubation period.

Measurements of minimum inhibitory concentration (MIC)

Standard broth microdilution assays, conducted according to CLSI guidelines,[28,29] were used to determine the minimal inhibitory concentration (MIC) of cationic polymer derivatives against gram-positive *Staphylococcus aureus* (*S. aureus*) ATCC 29213, gram-negative *Acinetobacter baumannii* (*A. baumannii*) ATCC 17978 and *Pseudomonas aeruginosa* (*P. aeruginosa*) ATCC 27853. Culture of each strain was adjusted to a 0.5 McFarland standard, equivalent to 1.5×10^8 CFU mL^{-1} before a further 1 : 100 dilution ($\sim 10^6$ CFU mL^{-1}) in cation-adjusted Mueller–Hinton broth (CAMHB) prior to addition in the assay well-plates. Serially diluted polymer solutions in CAMHB (100 μL) were added to polystyrene 96-well plates (Technoplas, Australia) with 100 μL of bacterial inoculum already contained in each well, giving final polymer concentrations ranging from 8–1024 μg mL^{-1} measured against each bacterial strain. Negative controls were incorporated by adding culture media with no bacteria or polymer present and positive controls contained only bacteria with no polymer added. Well-plates were incubated for 16–20 h at 37 °C after which MIC values were determined as the lowest polymer concentration where bacterial growth was not visibly detected.

Haemolysis assay

The effect of polymers on human red blood cells (HRBCs) (Australian Red Cross Blood Lifeblood, Australia) were measured.[30] A series of 2-fold dilutions of the polymer in PBS buffer were prepared to give the range of tested polymer concentrations. Fresh 5 mL aliquots of HRBC suspension were washed twice with PBS buffer, a process involving suspension in PBS and subsequent harvesting by centrifugation at 1000 *g* at 4 °C for 5 minutes. Resulting HRBC pellets were redispersed in PBS buffer to reach an overall HRBC concentration of 8% (v/v). Aliquots of this HRBC suspension (100 μL) were added to a 96-well plate before addition of each polymer solution (100 μL) to give final polymer concentrations of 0, 8, 16, 32, 64, 128, 256, 512, 1024 μg mL^{-1}. A negative control of PBS only (blank) and a positive control of HRBC immersed in 1% (v/v) Triton X-100 in PBS were incorporated alongside polymer/HRBC samples and four replicates were used for each sample condition. After the well-plates were incubated at 37 °C for 60 min, the plates were centrifuged at 1000*g* for 5 minutes. Supernatants of each sample were carefully withdrawn (as 100 μL volumes) and transferred to corresponding wells of a separate 96-well plate. The absorbance at 450 nm was measured with a microplate reader and percentage haemolysis was calculated according to eqn (2) using mean absorbance (Abs) readings for each sample.

$$\%\ \text{Haemolysis} = (\text{Abs sample} - \text{Abs blank})/(\text{Abs Triton-X} - \text{Abs blank}) \quad (2)$$

Results and discussion

Cationic poly(4-vinyl-*N*-methylpyridinium iodide-*co*-*N*-alkyl-maleimide) synthesis

Arising from the overarching goal to test the ability of novel cationic polymeric materials to selectively disrupt biological membranes and form nanodiscs, the synthesis of precursor monomers and RAFT functionalised copolymers was pursued. This process eventually yielded cationic copolymers imbued with hydrophobic *N*-alkyl-maleimide and hydrophilic 4-vinyl-*N*-methylpyridinium iodide units (the basic chemical structure of which is provided in Fig. 1B). The chosen polymerisation strategy combined pre-synthesised or purchased *N*-alkyl maleimides, such *N*-alkyl groups increased in their hydrophobicity ascending from methyl, ethyl, *n*-propyl, iso-butyl to *n*-butyl, with 4-vinyl pyridine (4VP) monomer units *via* a one-step RAFT polymerisation process.[23–25] Excess iodomethane was then

 This journal is © The Royal Society of Chemistry 2023

Published on 18 July 2023. Downloaded by University of Alberta on 8/1/2023 12:02:35 PM.

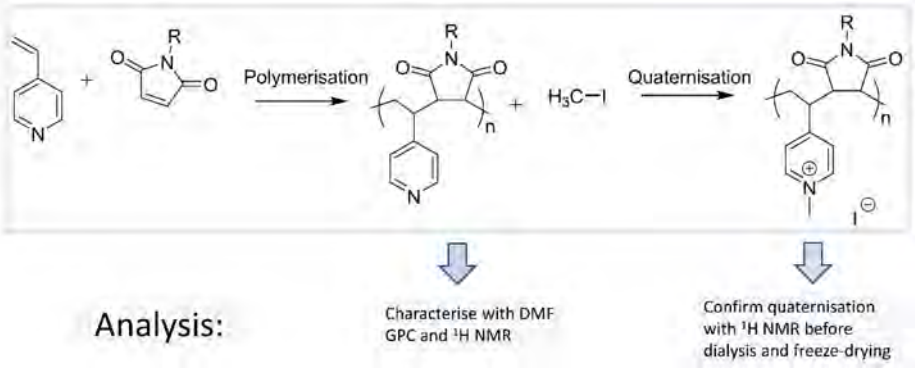

Scheme 1 Synthetic pathway for cationic poly(4-vinyl-*N*-methylpyridinium iodide-*co*-*N*-alkyl-maleimides) entailing a polymerisation followed by quaternisation *via* iodomethane addition.

added to the resultant poly(4-vinylpyridine-*co*-*N*-alkyl-maleimide) to quaternise the polymer into cationic poly(4-vinyl-*N*-methylpyridinium iodide-*co*-*N*-alkyl maleimide) (poly(MVP-*co*-AlkylM) according to Scheme 1.

The chosen strategy for poly(4-vinylpyridine-*co*-*N*-alkyl maleimide) synthesis saw percentage conversions of the 4VP component ranging between 60–80% (conversion values with respect to individual polymers are outlined in the Experimental section) according to ^{1}H NMR analysis. As shown in Table 1, GPC analysis showed dispersities ($Đ$) between 1.22–1.52 confirming the controlled chain growth of the RAFT mediated polymerisations, while ^{1}H NMR of the purified polymer products revealed a monomer ratio which can be approximated for all polymer variants to 1 : 1 4VP : AlkylM and therefore to 1 : 1 MVP : AlkylM post quaternisation. Naturally alternating polymer sequences were inferred due to the resistance of each monomer type (maleimides and vinylpyridines) to homopolymerisation.[31,32]

Successful quaternisation was confirmed by comparing ^{1}H NMR spectra of polymers before and after the addition of iodomethane (as is shown in Fig. S1–S7†). A broad peak emerged at around 4.5 ppm which was attributed to the *N*-methyl addition to the pyridine and peaks previously assigned to aromatic protons at ~7 and ~8.5 ppm, were shifted downfield to ~8 and ~9 ppm by the 4VP to MVP monomer functionalisation (as is displayed for respective *N*-alkyl maleimide derivatives in Fig. S3–S7†).

The number averaged molecular weights (M_n) of cationic copolymers estimated with ^{1}H NMR were in close agreement between each other ranging from 11 500 to 13 300 Da as shown in Table 1. Given the proximity between polymer molecular weights, monomer ratios and zeta potential measurements (ranging between +40 to +50 mV in Fig. S8†) for cationic polymer derivatives, reasonable comparison could then be made based on the length and hydrophobicity of the alkyl group attached to the maleimide unit. Thus, a systematic understanding of how selective membrane activity, nanodisc assembly and associated nanodisc properties are modulated by the alkyl substituent can be gained. Thus, a systematic understanding of how selective membrane activity, nanodisc assembly and associated nanodisc properties are modulated by the extent of the alkyl substituent can be gained.

Table 1 Parameter summary of RAFT synthesised cationic poly(*N*-methyl-4-vinyl pyridinium iodide-*co*-*N*-alkyl-maleimides) using ^{1}H NMR integral analysis of cationic derivatives to obtain MVP : AlkylM ratio and M_n as well as GPC (DMF) analysis to determine M_n, M_w and $Đ$ of the poly (4-vinyl pyridine-*co*-*N*-alkyl-maleimide (4VP-*co*-AlkylM) precursor polymer. Units of M_n and M_w are in Daltons

			GPC (4VP-*co*-AlkylM precursor)		
Copolymer	MVP : AlkylM	M_n (^{1}H NMR)	M_n	M_w	$Đ$
Poly(MVP-*co*-MM)	1.0 : 1.0	13 300	6700	10 000	1.49
Poly(MVP-*co*-EtM)	1.0 : 1.2	13 100	5600	7400	1.31
Poly(MVP-*co*-PM)	1.0 : 1.1	12 900	6200	7500	1.22
Poly(MVP-*co*-IBM)	1.1 : 1.0	11 700	6300	8500	1.33
Poly(MVP-*co*-BM)	1.0 : 1.2	11 500	5300	8100	1.52

Comparison of membrane solubilisation efficiency

Upon incubating cationic polymers with DMPC LUVs (0.1 μm diameter) in proportions of 0.2 : 1 polymer : lipid at 26 °C ± 1 °C (above the phase transition temperature of DMPC, T_m = 24 °C), a clear trend between the degree of hydrophobicity of the *N*-alkyl substituent and the DMPC solubilisation efficiency of polymers emerged from solution ^{31}P NMR spectra. The more extended the hydrocarbon substituent, the greater the prominence of a broad isotropic peak at approximately −1.0 ppm indicating DMPC LUVs conversion into polymer–lipid nanoparticles. This peak was not observed for large unilamellar liposomes which possess a slower tumbling rate conferred by their larger size, thus preventing a phosphorus signal being resolved on the NMR timescale (refer to Fig. 2A illustration of nanodiscs tumbling in solution).[33,34] As is captured in Fig. 2B–F, poly(MVP-*co*-MM) shows no nanodisc peak, poly (MVP-*co*-EtM) and poly(MVP-*co*-PM) show a slight peak at −1.0 ppm with heightened peak intensity for the *N*-propyl variant. Poly(MVP-*co*-IBM) elicits a yet more dominant peak and poly(MVP-*co*-BM), the derivative bearing the most extended alkyl chain, demonstrates the sharpest and most

Published on 18 July 2023. Downloaded by University of Alberta on 8/1/2023 12:02:35 PM.

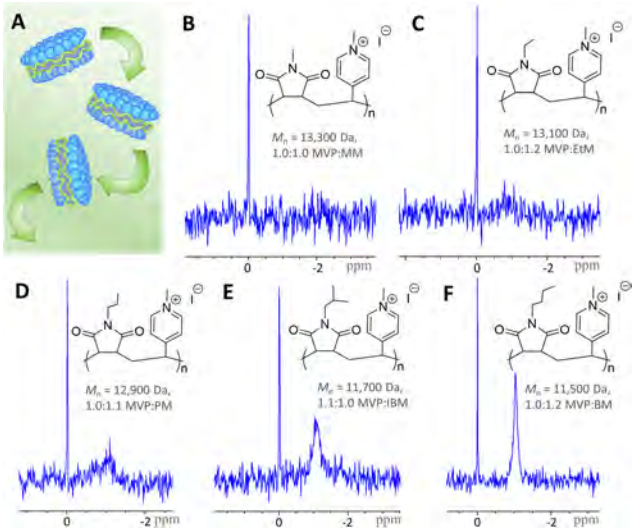

Fig. 2 (A) Illustration of a nanodisc tumbling in solution, ^{31}P NMR spectra of (B) poly(MVP-*co*-MM), (C) poly(MVP-*co*-EtM), (D) poly(MVP-*co*-PM), (E) poly(MVP-*co*-IBM) and (F) poly(MVP-*co*-BM), post incubation with DMPC LUVs in a 0.2 : 1 polymer : lipid molar ratio.

intense nanodisc peak. Lipid solubilisation was thereby found to increase along with hydrocarbon chain length of the maleimide *N*-substituent for this novel class of nanodisc assembling cationic polymer. It is worth noting that comparison of ^{31}P NMR solubilisation data between different polymers is a relatively crude measure with nanodisc size (which is likely to differ between cationic polymer versions) influencing nanodisc peak sharpness.[35] Nonetheless, the established shrinkage of polymer nanodisc size with increasing polymer : lipid ratio[36,37] along with knowledge that SMALP formation is thermodynamically driven by hydrophobic styrene unit insertion between lipid tail groups,[14] suggests that the greater propensity for longer alkyl chains to bury inside membranes, giving an increased overall polymer–lipid interaction, is a determining factor in not only increased liposome solubilisation efficiency, but may also be linked to a smaller nanodisc size.

Systematic study of cationic poly(MVP-*co*-AlkylM) nanodisc size and shape

Using the more hydrophobic cationic polymer derivatives (poly(MVP-*co*-PM), poly(MVP-*co*-IBM) and poly(MVP-*co*-BM)) shown to effectively extract phospholipids into nanodiscs, DLS and TEM were employed to measure the size distributions of 0.1 : 1 and 0.2 : 1 polymer : lipid samples directly after polymer incubation with 0.2 μm LUVs at 26 °C for 24 h without centrifugation. It was revealed that, in agreement with well-reported polymer nanodisc behaviour,[36–38] the higher polymer to lipid ratios produced smaller nanodiscs which was indicated by volume and intensity weighted DLS size-frequency distributions where the smaller nanodisc peak (peak # 1) consistently shifted to the left from 0.1 : 1 polymer : lipid (highlighted in blue in Fig. 3A–C) to 0.2 : 1 polymer : lipid (in pink in Fig. 3A–C) for all polymers evaluated (fitted DLS autocorrelation functions are provided in Fig. S9–S14†). Larger size populations revealed in DLS size-frequency distributions are expected to comprise a mixture of intact liposomes, polymer lipid nanodisc intermediate structures and polymer aggregates.[10] TEM sample images along with accompanying particle diameter histograms reinforced the nanodisc size dependence on polymer : lipid ratio (in Fig. S15–S17†). Interestingly, the more hydrophobic polymer variants gave way to smaller sized nanodiscs at equivalent polymer : lipid ratios. Comparison of DLS size-frequency distributions revealed poly(MVP-*co*-BM) assembling the smallest nanodiscs of 12.5 nm diameter (at 0.2 : 1 polymer : lipid) according to the smallest size-population peak (peak # 1) from intensity weighted distributions (refer to Fig. 3 and S12†). Poly(MVP-*co*-IBM) and poly(MVP-*co*-PM) respectively generated peak # 1 diameters of 22.1 nm and 47.1 nm from DLS data of 0.2 : 1 polymer : lipid samples. Likewise, for 0.1 : 1 polymer : lipid samples, the trend of smaller nanodisc size with increasing hydrophobicity was observed (the intensity weighted peak # 1 diameters were 18.9 nm, 31.9 nm and 33.8 nm for poly(MVP-*co*-BM), poly(MVP-*co*-IBM) and poly(MVP-*co*-PM), respectively). Similarly, TEM images and acquired histograms in Fig. 4. Supported the relationship between nanodisc size and polymer hydrophobicity for 0.1 : 1 polymer : lipid samples comparing BM, IBM and PM cationic derivatives.

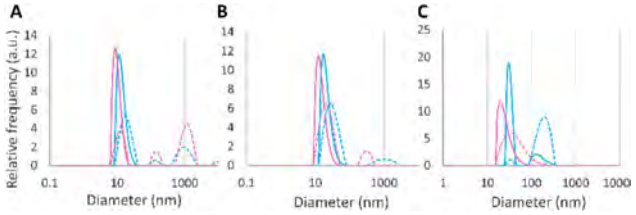

Fig. 3 DLS particle size frequency distribution graphs weighted by intensity of scattered light (dotted lines) and volume fraction occupied by particles (solid lines) of (A) poly(MVP-*co*-BM), (B) poly(MVP-*co*-IBM) and (C) poly(MVP-*co*-PM) incubated with DMPC LUVs in a 0.1 : 1 polymer : lipid molar ratio (blue) and in a 0.2 : 1 polymer : lipid molar ratio (pink).

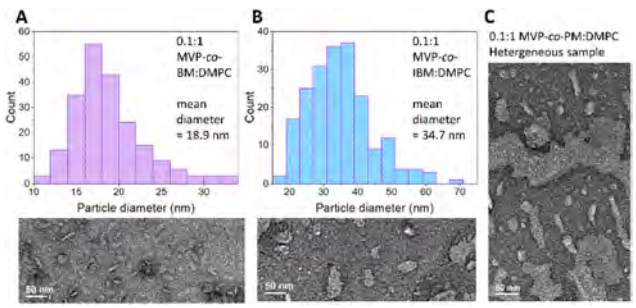

Fig. 4 TEM derived histograms (constructed using imageJ analysis of at least 100 particles across two different axes) and accompanying images of polymer derivates combined with DMPC LUVs in 0.1 : 1 polymer : lipid molar ratios for (A) poly(MVP-*co*-BM), (B) poly(MVP-*co*-IBM) and (C) poly(MVP-*co*-PM) (for which no histogram was constructed). The scale of TEM micrographs is 50 nm.

This journal is © The Royal Society of Chemistry 2023

Published on 18 July 2023. Downloaded by University of Alberta on 8/1/2023 12:02:35 PM.

The clarity of this trend was somewhat obscured by TEM data from 0.2 : 1 polymer : lipid samples (summarised in Table S1†). Poly(MVP-*co*-BM), poly(MVP-*co*-IBM) and poly(MVP-*co*-PM) gave respective diameters of 14.1 nm, 10.5 nm and 14.5 nm for 0.2 : 1 polymer : lipid ratio samples. These particle size similarities suggest that nanodisc size dependence on polymer hydrophobicity becomes negligible for higher polymer : lipid ratios. The combined effects of a small sample size in statistical analysis, particle crowding evident from 0.2 : 1 polymer : lipid TEM images and marginal differences in nanodisc particle size, which were likely to have been magnified by the DLS bias towards larger particle scattering,[39] are thought to have resulted in the discrepancy between TEM and DLS data for these samples.

Capabilities to tilt the TEM sample stage using the α-tilt function to manipulate the angle the electron beam interacts with the plane of the grid surface, permits the opportunity to observe disc particle shape. Disc-shaped nanoparticles appear circular or elliptical on the non-tilted grid-surface (0° α-tilt) and become skinnier and rod-like when viewed from an angle more adjacent to the grid surface plane (45–60° α-tilt).[40] Fig. 5A captures an individual nanodisc particle formed from poly(MVP-*co*-BM) (0.1 : 1 polymer : DMPC) appearing round and elliptical measuring 14.87 nm across the horizontal axis at 0° α-tilt which then becomes pin-like in Fig. 5B measuring 4.04 nm, the approximate thickness of a phospholipid bilayer, across the horizontal axis and thus presenting a single nanodisc viewed from the rim edge. Analogous observations were made for poly(MVP-*co*-IBM) nanodiscs (in Fig. S18†).

SAXS data obtained for poly(MVP-*co*-BM) and for RAFT synthesised SMA (D10) 0.2 : 1 polymer : lipid samples (the latter was selected as a benchmark reference for polymer/lipid nanodiscs) supports the structural arrangement of lipid-nanodiscs by exhibiting the signature double peak *I*(q) *vs*. q plot pattern for the two surveyed sample concentrations displayed in Fig. 6A and B (SAXS data for polymer only controls are provided in Fig. S19–S21† as a reference).[41,42] These plots exhibited two broad peaks and showed a local minimum at medium to high q between 0.05–0.08 $Å^{-1}$ resulting from the negative scattering length density of hydrophobic lipid tails within the DMPC bilayer core giving rise to a core–shell contrast situation.

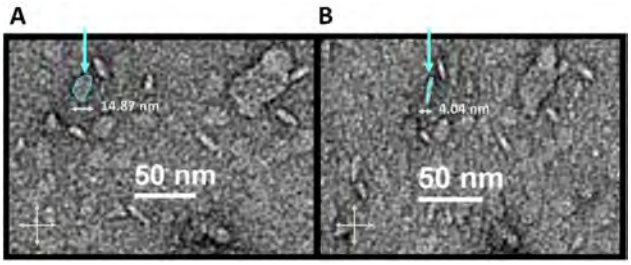

Fig. 5 Comparison between TEM image of poly(MVP-*co*-BM) added to DMPC 0.1 : 1 polymer : lipid molar ratio at (A) 0 degrees sample stage α-tilt and at (B) 55 degrees sample stage α-tilt. The same particle has been measured along the horizontal axis as 14.87 nm at 0 degrees α-tilt and 4.04 nm at 55 degrees α-tilt. The scale is 50 nm.

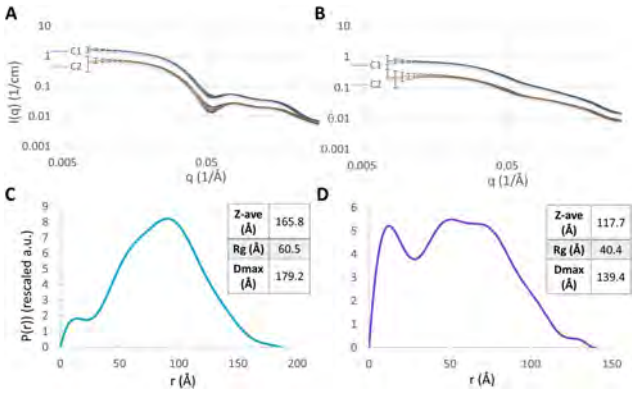

Fig. 6 SAXS *I*(q) *versus* q plots for (A) diblock SMA (D10) and (B) poly (MVP-*co*-BM) added to DMPC 0.2 μm LUVs (0.2 : 1 polymer to DMPC molar ratio) at DMPC concentration of 5.6 mM and polymer concentration of 1.1 mM (C1) and C1 diluted 2-fold (C2). Accompanying *P*(r) functions of (C) diblock SMA (D10) added to DMPC LUVs (0.2 : 1 polymer to DMPC) at C2 and (D) poly(MVP-*co*-BM) added to DMPC LUVs (0.2 : 1 polymer to DMPC) at C2. Zeta average diameter (Z-Ave) was collected from DLS, radius of gyration (R_g) was extracted from Guinier analysis of SAXS data and D_{max} was given by the *P*(r) function intercept.

Nanodisc contrast with respect to SAXS scattering also affected the *P*(r) functions of Fig. 6C and D acquired by indirect Fourier transform (IFT) wherein local minima at ~15–30 Å interrupt the smooth singular peak expected for disc-shaped particles for both poly(MVP-*co*-BM) and SMA (D10) nanodiscs. On the basis of the aforementioned *I*(q) *vs.* q plot and *P*(r) function features, this data demonstrates a qualitative agreement with data reported for SMALPs and MSP1D1 nanodiscs.[41]

Using Guinier analysis conducted on PRIMUS, the radius of gyration (R_g) was determined and the maximum diameter (D_{max}) of the particles was derived from the GNOM executed *P*(r) functions which are both summarized in Fig. 6C and D. Agreement between DLS measured zeta-average (Z-ave) diameter taken from diluted SAXS samples and the D_{max} values calculated from SAXS served to corroborate the aforementioned fundamental size and shape information for novel cationic polymer nanodiscs.

Effects of cationic polymer nanodisc composition on lipid bilayer integrity and physical properties

Various biophysical techniques can offer insight into the physical properties of phospholipid bilayers including advanced NMR,[43] differential scanning calorimetry (DSC)[44] and fluorescence based approaches.[45] The solvatochromic Laurdan fluorescent probe offers a simple and highly sensitive method to detect membrane phase changes due to the red shift of the Laurdan's emission spectrum when immersed within more disordered membrane environments.[45,46] Temperature dependent emission spectra and generalized polarization (GP) values calculated with eqn (1) were acquired for DMPC : Laurdan (100 : 1) 0.1 μm LUV samples, the emission spectra of which are presented from 10–50 °C in increments of 5 °C in Fig. 7A. A shift in the emission maximum

Published on 18 July 2023. Downloaded by University of Alberta on 8/1/2023 12:02:35 PM.

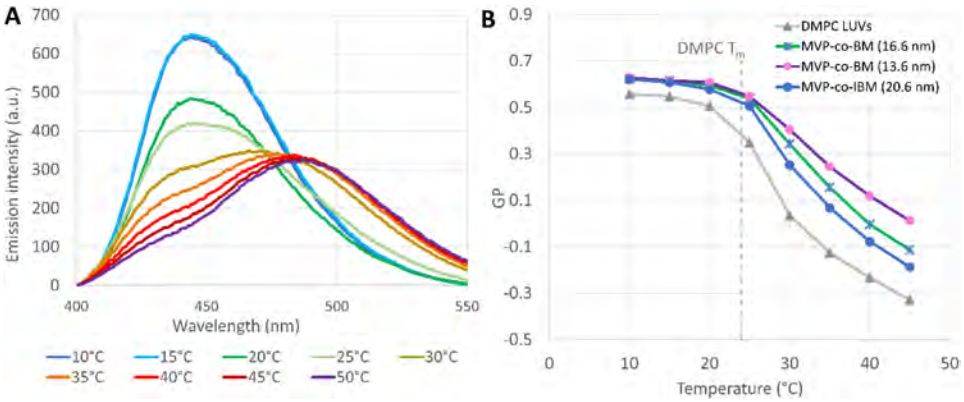

Fig. 7 (A) Overlayed emission spectra of DMPC : Laurdan (100 : 1) LUVs from 10 to 50 °C in 5 °C temperature increments and (B) generalised polarisation (GP) *versus* temperature (from 10 to 45 °C) for DMPC : Laurdan (100 : 1) LUVs (in grey), in green poly(MVP-*co*-BM) incubated with DMPC : Laurdan (100 : 1) LUVs in a 0.1 : 1 polymer : lipid molar ratio (diameter = 16.6 nm), in purple (MVP-*co*-BM) incubated with DMPC : Laurdan (100 : 1) LUVs in a 0.2 : 1 polymer : lipid molar ratio (diameter = 13.6 nm) and in blue poly(MVP-*co*-IBM) added to DMPC : Laurdan (100 : 1) LUVs in a 0.2 : 1 polymer : lipid molar ratio (diameter = 20.6 nm).

from ≈440 nm to ≈480 nm before and after the gel-to-liquid phase transition temperature (T_m) for Laurdan containing DMPC LUVs is due to increased solvent relaxation, resulting from greater penetration of the lipid membrane by polar solvent molecules when the lipid bilayers become more disordered.[45] Liposome only samples were compared against purified cationic polymer nanodiscs of poly(MVP-*co*-BM) assembled from 0.1 : 1 polymer : lipid and poly(MVP-*co*-BM/IBM) assembled from 0.2 : 1 polymer : lipid ratios formed from lipid mixtures composed of DMPC : Laurdan (100 : 1). Prior to Laurdan fluorescence, nanodisc samples were measured with DLS to determine their relative size; poly(MVP-*co*-IBM) 0.2 : 1 polymer : lipid gave a size of 20.6 nm, poly(MVP-*co*-BM) 0.1 : 1 polymer : lipid gave 16.6 nm nanodiscs and poly(MVP-*co*-BM) 0.2 : 1 polymer : lipid gave the smallest disc size of 13.6 nm.

GP against temperature plots in Fig. 7B revealed a size-dependence of the steepness of the inflection point occurring after the DMPC phase transition temperature (T_m = 24 °C). Smaller nanodiscs demonstrated a shallower dip in GP with increased temperature implying that constituent lipid bilayers in smaller nanodiscs were more constrained and ordered above the T_m. We postulate that this effect is largely due to the larger area interface of polymer and lipid interaction for smaller nanodiscs where more lipids are in contact with or in proximity to the encircling polymer, thereby reducing the cooperativity and extent of the DMPC phase transition from ordered gel to liquid crystalline phase.[41,47] Also apparent from GP *vs.* temperature plots, was that the phase transition of smaller cationic polymer nanodiscs in particular took place over a broader temperature range compared to DMPC LUVs; inferred from a more gradual drop in GP evident after 25 °C for nanodisc samples. Similar heightened lipid order and reduced T_m cooperativity has been reported for SMA nanodiscs compared to liposomes,[48] although the dependence of lipid bilayer rigidity on polymer nanodisc size has been largely overlooked.

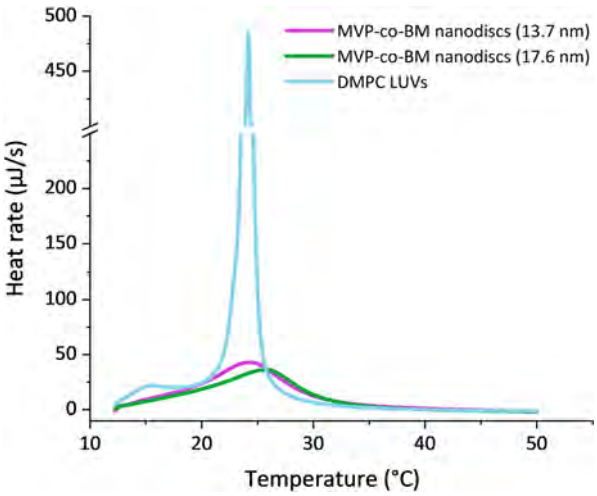

Fig. 8 DSC thermograms showing the heat rate (μJ s^{-1}) of 7.14 mM DMPC initially in the form of 0.1 μm LUVs (in blue) upon incubation with 0.2 molar fraction of poly(MVP-*co*-BM) polymer to form 13.7 nm nanodiscs (purple) and with 0.1 molar fraction of poly(MVP-*co*-BM) to form 17.6 nm nanodiscs (green). Phase-transition temperature (T_m) values are summarised for each sample.

Broadening of the DMPC gel-to-liquid phase transition for membranes stabilised by cationic polymer nanodiscs compared to 0.1 μm LUVs was also evident in complimentary differential scanning calorimetry (DSC) thermograms (in Fig. 8 and Fig. S22†). DMPC containing poly(MVP-*co*-BM) nanodiscs were compared with LUVs at 0.1 : 1 and 0.2 : 1 polymer : lipid molar ratios which produced respective DLS measured particle sizes of 17.6 nm and 13.7 nm. The initial upward jolt in T_m (to 25.8 °C) at the lower polymer : lipid ratio of 0.1 : 1 poly(MVP-*co*-BM) : DMPC before reverting to a slightly lower T_m (24.4 °C) at the increased 0.2 : 1 polymer : lipid ratio and smaller disc size was consistent with the findings of Grethen and coworkers,[38]

 This journal is © The Royal Society of Chemistry 2023

Published on 18 July 2023. Downloaded by University of Alberta on 8/1/2023 12:02:35 PM.

which used DSC to observe the phase-transition behaviour of SMALPS formed by a wide range of SMA : DMPC molar ratios. They discovered that, in contrast with to membrane scaffold protein (MSP) nanodiscs which shift the T_m to higher temperatures, SMALPs slightly heighten the T_m compared to LUVs at low polymer : lipid (mol : mol) and then reduce the T_m at 0.31–1.04 polymer : lipid ratios, which are well above the $R_S^{m,SOL}$ = 0.13 value required for complete DMPC lipid solubilisation by SMA (2 : 1). Thus, a more fluid and loosely packed acyl-chain core is attributed to polymer nanodiscs at higher polymer : lipid ratios at temperatures below the T_m, which can be rationalised by the increased interaction between intercalating polymer and lipid. We did not investigate such high polymer : lipid ratios to fully observe this trend for poly(MVP-*co*-AlkylM)s, although we observed a similar effect for the polymer : lipid ratios measured. A distinct advantage of temperature-dependent Laurdan fluorescence compared with DSC is the ability to monitor lipid-bilayer order at temperatures higher than the gel-to-liquid phase transition.[46,49] As was previously shown by Laurdan fluorescence analysis, the smaller poly(MVP-*co*-BM) or poly(MVP-*co*-IBM) nanodisc size results in greater perturbation of lipid bilayer physical properties where lipids were found to be more constrained and ordered in the liquid phase. Given the somewhat counterintuitive lowering of the phase transition temperature and the increased lipid ordering in the liquid phase in smaller polymer nanodiscs,[38] it is helpful to consider the analogous impact of cholesterol on membrane physical properties, which also intercalates between the lipid acyl chains and facilitates the coexistence of high membrane fluidity and tight packing of lipid molecules.[50,51] Much like cholesterol, polymer nanodisc materials show a lowering of the gel-to-liquid phase transition whilst resulting in a more ordered lipid bilayer in the liquid phase, an effect which is more pronounced at higher molar fractions of polymer.

Membrane disruption selectivity shown across cationic poly (MVP-*co*-AlkylM) derivatives

The impact of systematically increasing the hydrophobicity of the maleimide *N*-substituent (from methyl to butyl), was hypothesised to increase the overall membrane disruption by polymers irrespective of membrane type. Whereas the less hydrophobic derivates were speculated to show a weaker overall membrane disruption and furthermore, to enact preferential disruption of more negatively charged membrane surfaces due to their cationic monomer component. Systematic dye-release assays were undertaken, to both investigate these hypotheses and to explore the potential for bacterial membrane selectivity in novel cationic polymers.

Each cationic poly(MVP-*co*-AlkylM) variant was added to fluorescent dye-loaded 0.1 μm LUVs of varying membrane composition across a spectrum of polymer concentrations observed to capture the full range of activity, prior to the ultimate addition of Triton X-100 prompting 100% dye release, a process illustrated in Fig. 9B (all % dye-release against time data traces can be found in Fig. S23–S26† and complimentary UV absorption spectra of polymers are shown in Fig. S27† exhibiting absorbances below the 485 nm excitation wavelength). Phospholipid mixtures spanned from eukaryotic mimetic systems POPC and POPC : POPG (4 : 1)[21] to gram-positive *S. aureus* mimetic POPC : POPG (1 : 1)[52] and gram-negative *E. coli* membrane simulant POPE : POPG : CL (15 : 4 : 1).[53] As Fig. 9A reflects, the extent of *E. coli* mimetic membrane disruption was directly connected to the hydrophobicity of the maleimide *N*-alkyl substituent with methyl, ethyl, propyl, isobutyl and butyl derivates showing respective maximum dye-release values of 19%, 21%, 41%, 60% and 87% rounded to the nearest integer. POPE and CL containing phospholipid mixtures were previously reported to resist amphiphilic SMA polymer insertion and solubilisation owing to their intrinsic

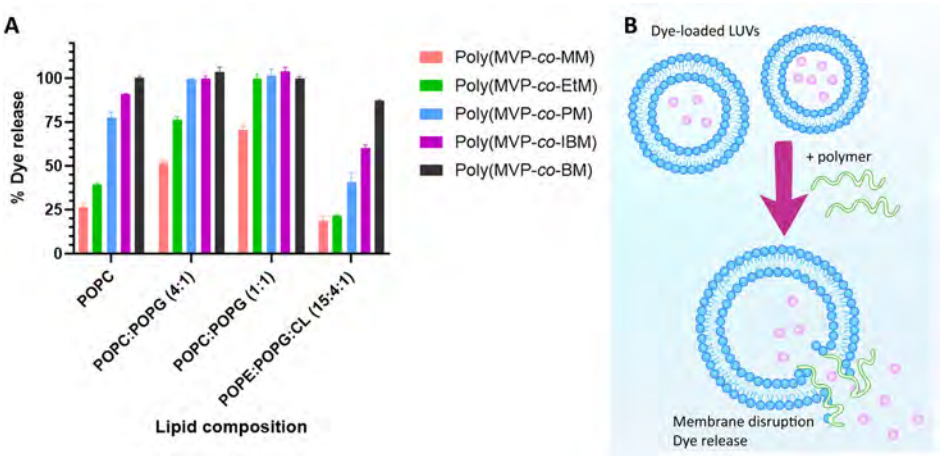

Fig. 9 (A) Column graph comparing the maximum % dye-release over time after addition of cationic poly(MVP-*co*-MM or EtM or PM or IBM or BM) to CF dye-loaded LUVs comprised of POPC, POPC : POPG (4 : 1), POPC : POPG (1 : 1) and POPE : POPG : CL (15 : 4 : 1) lipid compositions. In (B), a schematic representation of the dye-release assay experimental procedure.

Published on 18 July 2023. Downloaded by University of Alberta on 8/1/2023 12:02:35 PM.

negative curvature which induces increased lateral pressure in the acyl chain region of membranes.[10,19] These effects are reiterated in the dye-leakage profile of the *E. coli* mimetic LUVs in comparison to other membrane compositions solely comprised of cylindrical shaped POPC and POPG lipids displayed in Fig. 9A. Despite the qualitative distinctness in membrane composition, a graduated incline in membrane disruption with longer alkyl substituent chain length was likewise found for the simpler and more disruption prone POPC LUV system, wherein maximum dye-releases of 26%, 39%, 78%, 91% and 100% were recorded from methyl-through to butyl-bearing polymers in order of increasing hydrophobicity. As the anionic POPG fraction of POPC : POPG LUV mixtures was systematically increased from POPC to POPC : POPG (4 : 1) through to POPC : POPG (1 : 1), thereby further resembling the charge of bacterial membrane surfaces, less hydrophobic and more weakly interacting cationic copolymers of poly(MVP-*co*-MM), poly(MVP-*co*-EtM) and poly(MVP-*co*-PM) markedly increased in their membrane disruption capacity as is shown in Fig. 9A. Poly(MVP-*co*-EtM) showed the greatest selectivity between membrane types, initiating 39% maximum dye release against POPC LUVs, 76% maximum dye release against POPC : POPG (4 : 1) and 100% dye release against POPC : POPG (1 : 1).

Capacities for membrane disruption exhibited by poly(MVP-*co*-AlkylM) polymers, monitored by dye-release assays, do not imply the evolution of nanodiscs or nanoscale structures. In fact, there was no nanodisc formation for methyl, ethyl or propyl derivates added to POPC or POPC : POPG (1 : 1) membranes according to ^{31}P NMR and TEM analysis of 0.2 : 1 polymer : lipid samples (supported by Fig. S28–S30†). Whereas nanodiscs were able to be formed from these membrane systems for more hydrophobic derivatives and, in line with prevailing trends, nanodisc yield was markedly higher for poly(MVP-*co*-IBM) added to POPC : POPG (1 : 1) compared to POPC only membranes at 0.2 : 1 polymer : lipid ratios (refer to Fig. S31†). It can be claimed that although membrane disruption does not directly map to nanodisc formation, there is a correlation for the most strongly disrupting cationic polymer derivates, which is coherent with previous work establishing membrane insertion as a critical process in the mechanism of polymer nanodisc assembly.[10,54] Such selective membrane interaction and preferential disruption by less hydrophobic cationic polymers against membranes with anionic surfaces provides a theoretical framework for polymer design towards a plethora of applications including selective membrane component solubilisation, biosensing and antimicrobial development.

Poly(MVP-*co*-AlkylM) selective inhibition of bacterial growth

Antimicrobial activity was further investigated with respect to methyl, ethyl, propyl and butyl poly(MVP-*co*-AlkylM) polymers. Disk diffusion assay (DDA) was first performed to assess the inhibition of bacterial cell growth in agar inoculated with either gram-positive *S. aureus* ATCC 29213 or gram-negative *A. baumannii* ATCC 17978. At high polymer concentrations

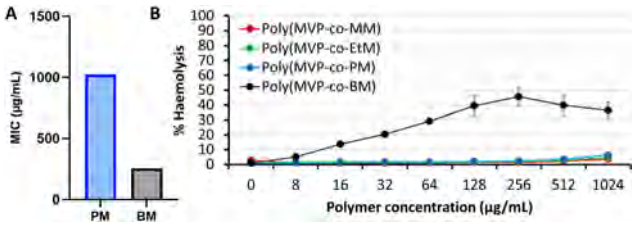

Fig. 10 Poly(MVP-*co*-PM) (PM) and poly(MVP-*co*-BM) (BM) demonstrated MIC endpoint values which are graphically represented in (A) against *A. baumannii* ATCC 17978 and *S. aureus* ATCC 29213. Haemolysis assay findings in (B) show plots for % haemolysis for polymers poly(MVP-*co*-MM), poly(MVP-*co*-EtM), poly(MVP-*co*-PM) and poly(MVP-*co*-BM) across their tested polymer concentration range from 0–1024 μg mL^{-1}.

against *S. aureus* (5 mg per disc) and *A. baumannii* (2.5 mg and 5 mg per disc), distinct zones of inhibition were observed, except for poly(MVP-*co*-MM) against *A. baumannii* for which no inhibition was shown (DDA data are displayed in Fig. S32†). Having verified the potential to inhibit bacterial growth of different cell types, minimum inhibitory concentrations (MICs) were measured to define the lowest polymer concentration values where bacterial growth was no longer detectable. Represented in Fig. 10A and B, poly(MVP-*co*-PM) generated MICs of 1024 μg mL^{-1} against both *S. aureus* and *A. baumannii* and, in line with trends gleaned from earlier dye release assays, the more hydrophobic poly(MVP-*co*-BM) displayed lower MICs of 256 μg mL^{-1} against both *S. aureus* and *A. baumannii*. Conversely, the MICs for methyl and ethyl poly(MVP-*co*-AlkylM) polymers were beyond the range of measurement with respect to either strain (MIC > 1024 μg mL^{-1}), and no polymers produced an MIC value within the measurement range against the *P. aeruginosa* ATCC 27853 control (all MIC values are summarised in Table S2†) which is likely due to poor permeability of its outer membrane.[55]

While the MICs obtained for propyl and butyl poly(MVP-*co*-AlkylM) derivatives are orders of magnitude above that required for standard antibiotic drugs,[56,57] complimentary haemolysis experiments revealed that poly(MVP-*co*-PM) showed minimal disruption of human red blood cells (HRBCs) across a concentration range up to 1024 μg mL^{-1}, which is the MIC required by poly(MVP-*co*-PM) to inhibit growth of *S. aureus* and *A. baumannii* strains. As such, poly(MVP-*co*-PM) elicited a maximum of 6% haemolysis at this MIC. Likewise, the weakly disrupting methyl and ethyl derivatives, in line with prior dye release experiments, expectedly gave way to negligible haemolysis. Poly(MVP-*co*-BM) showed a gradual incline in % haemolysis over the tested concentration range, peaking at 45% haemolysis at its MIC value (256 μg mL^{-1}) against the bacterial strains, before gently decreasing in haemolytic activity as reflected in Fig. 10B. The haemolysis peaking at 256 μg mL^{-1} may be the result of the poly(MVP-*co*-BM) polymers changing their structural arrangement in solution which may involve aggregating or forming micelles above their critical micelle concentration (CMC). It is commonplace that

 This journal is © The Royal Society of Chemistry 2023

Published on 18 July 2023. Downloaded by University of Alberta on 8/1/2023 12:02:35 PM.

HRBCs are employed to indicate the cytotoxicity and haemolytic effect of biocompatible materials.[58,59] From this perspective, the relative susceptibility of bacteria to poly(MVP-*co*-AlkylMs) compared to mammalian HRBCs can be optimised by the degree of *N*-alkyl hydrophobic extension with poly(MVP-*co*-PM) showing enhanced selectivity, suggesting that trends from dye release assays are translatable to native membrane systems. The hydrophobic optimisation of polymer membrane selectivity also offers insight into the tuning of polymer microbial membrane selectivity for more potent antimicrobial polymers.

Conclusions

The nature of polymer–lipid nanodisc assembly resulting from novel RAFT synthesised cationic polymers comprising hydrophobic alkyl (methyl, ethyl, *n*-propyl, *n*-butyl and iso-butyl) maleimide units and hydrophilic *N*-methyl-4-vinyl pyridinium iodide (MVP) after equilibration with DMPC large unilamellar vesicles was probed by ^{31}P NMR solution, DLS, TEM and SAXS studies. Lipid solubilisation efficiency was found to increase along with hydrocarbon chain length of the maleimide *N*-alkyl substituent. The relationship between the increased polymer : lipid ratio and nanodisc diameter shrinkage was confirmed and it was further discovered that the more hydrophobic polymer variants also gave way to smaller sized nanodiscs at equivalent polymer : lipid ratios. Overall phospholipid bilayer order of poly(MVP-*co*-IBM/BM) nanodiscs were investigated through temperature dependent Laurdan fluorescence and DSC. The cooperativity of the gel-to-liquid phase transition was reduced for nanodiscs compared to LUVs indicating the perturbation of uniform physical lipid packing and fluidity upon the introduction of polymer. DMPC lipid bilayers stabilised within smaller nanodiscs were more ordered and constrained above the T_m, indicating the ability to adjust physical properties of constituent lipids along with nanodisc size.

The selective disruption of membranes by poly(MVP-*co*-AlkylM) polymers, according to dye release assays, was affected by slight differences in polymer hydrophobicity. Shorter *N*-alkyl chain length polymers, particularly poly(MVP-*co*-EtM), exhibited relatively low activities against eukaryotic mimetic POPC membrane and increased their liposome disruption as POPC : POPG membrane mixtures increased in their anionic POPG component. The extent of this membrane selectivity was further explored using a combination of DDA, MIC and haemolysis assays. Although these polymers showed no therapeutically relevant antimicrobial selectivity, a relative susceptibility of gram-positive *S. aureus* and gram-negative *A. baumannii* bacterial strains to disruption by hydrophobic butyl- and propyl-cationic polymer poly(MVP-*co*-AlkylM) derivatives compared to mammalian HRBCs was shown. This effect was sensitive to the *N*-alkyl chain length with the less potent bacteriostatic poly(MVP-*co*-PM) derivative showing enhanced selectivity.

Preferential membrane interaction by less hydrophobic cationic polymers against membranes with anionic surfaces provides a theoretical framework for designing polymers towards applications including selective membrane component solubilisation, biosensing and antimicrobial development. These findings lend further merit to the concept that optimal selective cationic bacterial membrane disruptors must be finely balanced in their degree of hydrophobicity in both being enough to significantly promote membrane activity and not so much as to damage human cells and tissues. Although the potency of these compounds are not within a therapeutic range for antimicrobial applications, the membrane selectivity of poly(MVP-*co*-AlkylM) polymer materials characterised in this work could be further enhanced by current developments in nanoconjugation, wherein the attachment of various antimicrobials to metal nanoparticles has been shown to increase their inhibition of bacterial growth.[56] A vast spectrum of possible polymer morphologies and architectures, which can be assembled from the same monomer building blocks, has also allowed antimicrobial polymers to be significantly tuned and optimised.[21,60] Alternatively, attaching fluorescent pendant groups to selective polymers may allow for use as biosensors to differentiate membrane and cell types through preferential membrane binding and insertion.[61]

Author contributions

MDF: methodology, investigation, formal analysis, data curation, validation, visualization, conceptualization, writing – original draft and writing – review & editing. JZ: methodology, investigation, validation. AYJT: investigation, methodology, writing – review & editing. LvH: resources, formal analysis, validation, writing – review & editing. HHY: investigation, formal analysis, methodology, data curation. JL: resources, validation, conceptualisation, writing – review & editing. LLM: Supervision, conceptualisation, project administration, resources, funding acquisition, writing – review & editing. SHT: Supervision, conceptualisation, project administration, resources, funding acquisition, writing – review & editing.

Conflicts of interest

There are no conflicts to declare.

Acknowledgements

M. D. F. thanks Monash University for the award of her RTP stipend PhD scholarship. Special acknowledgement goes to Dr Alasdair McKay for help with ^{31}P NMR experiment optimisation, Prof. Louise Bennett for providing access to the fluorescent plate reader for dye-release assays, Assoc. Prof. Kellie Tuck for access to the fluorometer facilitating temperature-dependent fluorescence experiments and Dr Tina Hsia for her generously shared expertise and guidance in the practicals of

Published on 18 July 2023. Downloaded by University of Alberta on 8/1/2023 12:02:35 PM.

RAFT polymerisation and organic synthesis. The authors acknowledge the use of the instruments and scientific and technical assistance of Dr Tim Williams and Dr Russell King at the Monash Centre for Electron Microscopy, a Node of Microscopy Australia. This research was undertaken on the SAXS/WAXS (Small and Wide Angle X-ray Scattering) beamline at the Australian Synchrotron, part of ANSTO. Finally, S. H. T. would like to acknowledge the support by ARC Centre of Excellence for Enabling Eco-Efficient Beneficiation of Minerals (Grant No. CE200100009).

References

1 H. Yin and A. D. Flynn, *Annu. Rev. Biomed. Eng.*, 2016, **18**, 51–76.
2 H. H. Shen, T. Lithgow and L. Martin, *Int. J. Mol. Sci.*, 2013, **14**, 1589–1607.
3 M. J. Parmar, M. Lousa Cde, S. P. Muench, A. Goldman and V. L. Postis, *Biochem. Soc. Trans.*, 2016, **44**, 877–882.
4 M. D. Farrelly, L. L. Martin and S. H. Thang, *Chem. – Eur. J.*, 2021, **27**, 12922–12939.
5 F. Li, P. F. Egea, A. J. Vecchio, I. Asial, M. Gupta, J. Paulino, R. Bajaj, M. S. Dickinson, S. Ferguson-Miller, B. C. Monk and R. M. Stroud, *J. Biol. Chem.*, 2021, **296**, 100557.
6 C. Sun, S. Benlekbir, P. Venkatakrishnan, Y. Wang, S. Hong, J. Hosler, E. Tajkhorshid, J. L. Rubinstein and R. B. Gennis, *Nature*, 2018, **557**, 123–126.
7 W. Qiu, Z. Fu, G. G. Xu, R. A. Grassucci, Y. Zhang, J. Frank, W. A. Hendrickson and Y. Guo, *Proc. Natl. Acad. Sci. U. S. A.*, 2018, **115**, 12985–12990.
8 M. Peplow, *ACS Cent. Sci.*, 2020, **6**, 1274–1277.
9 C. Sun and R. B. Gennis, *Chem. Phys. Lipids*, 2019, **221**, 114–119.
10 S. Scheidelaar, M. C. Koorengevel, J. D. Pardo, J. D. Meeldijk, E. Breukink and J. A. Killian, *Biophys. J.*, 2015, **108**, 279–290.
11 J. F. Bada Juarez, J. C. Munoz-Garcia, R. Inacio Dos Reis, A. Henry, D. McMillan, M. Kriek, M. Wood, C. Vandenplas, Z. Sands, L. Castro, R. Taylor and A. Watts, *Biochim. Biophys. Acta, Biomembr.*, 2020, **1862**, 183152.
12 R. L. Grime, J. Goulding, R. Uddin, L. A. Stoddart, S. J. Hill, D. R. Poyner, S. J. Briddon and M. Wheatley, *Nanoscale*, 2020, **12**, 11518–11525.
13 T. J. Knowles, R. Finka, C. Smith, Y. Lin, T. Dafforn and M. Overduin, *J. Am. Chem. Soc.*, 2009, **131**, 7484–7485.
14 S. C. L. Hall, C. Tognoloni, G. J. Price, B. Klumperman, K. J. Edler, T. R. Dafforn and T. Arnold, *Biomacromolecules*, 2018, **19**, 761–772.
15 J. J. Dominguez Pardo, J. M. Dorr, A. Iyer, R. C. Cox, S. Scheidelaar, M. C. Koorengevel, V. Subramaniam and J. A. Killian, *Eur. Biophys. J.*, 2017, **46**, 91–101.
16 V. Postis, S. Rawson, J. K. Mitchell, S. C. Lee, R. A. Parslow, T. R. Dafforn, S. A. Baldwin and S. P. Muench, *Biochim. Biophys. Acta*, 2015, **1848**, 496–501.
17 C. Logez, M. Damian, C. Legros, C. Dupre, M. Guery, S. Mary, R. Wagner, C. M'Kadmi, O. Nosjean, B. Fould, J. Marie, J. A. Fehrentz, J. Martinez, G. Ferry, J. A. Boutin and J. L. Baneres, *Biochemistry*, 2016, **55**, 38–48.
18 M. T. Doyle, J. R. Jimah, T. Dowdy, S. I. Ohlemacher, M. Larion, J. E. Hinshaw and H. D. Bernstein, *Cell*, 2022, **185**, 1143–1156.
19 K. Janson, J. Zierath, F. L. Kyrilis, D. A. Semchonok, F. Hamdi, I. Skalidis, A. H. Kopf, M. Das, C. Kolar, M. Rasche, C. Vargas, S. Keller, P. L. Kastritis and A. Meister, *Biochim. Biophys. Acta, Biomembr.*, 2021, **1863**, 183725.
20 R. M. Epand and R. F. Epand, *Biochim. Biophys. Acta*, 2009, **1788**, 289–294.
21 Y. Jiang, W. Zheng, L. Kuang, H. Ma and H. Liang, *ACS Infect. Dis.*, 2017, **3**, 676–687.
22 L. Yu, K. Li, J. Zhang, H. Jin, A. Saleem, Q. Song, Q. Jia and P. Li, *ACS Appl. Bio Mater.*, 2022, **5**, 366–393.
23 J. Chiefari, Y. K. Chong, F. Ercole, J. Krstina, J. Jeffery, T. P. T. Le, R. T. A. Mayadunne, G. F. Meijs, C. L. Moad, G. Moad, E. Rizzardo and S. H. Thang, *Macromolecules*, 1998, **31**, 5559–5562.
24 G. Moad, E. Rizzardo and S. H. Thang, *Chem. – Asian J.*, 2013, **8**, 1634–1644.
25 G. Moad, E. Rizzardo and S. H. Thang, *Aust. J. Chem.*, 2012, **65**, 985–1076.
26 Q. Han, J. Binns, J. Zhai, X. Guo, T. M. Ryan, C. J. Drummond and T. L. Greaves, *J. Mol. Liq.*, 2022, **345**, 117816.
27 Y. Zhu, J. Lu, M. L. Han, X. Jiang, M. A. K. Azad, N. A. Patil, Y. W. Lin, J. Zhao, Y. Hu, H. H. Yu, K. Chen, J. D. Boyce, R. A. Dunstan, T. Lithgow, C. K. Barlow, W. Li, E. K. Schneider-Futschik, J. Wang, B. Gong, B. Sommer, D. J. Creek, J. Fu, L. Wang, F. Schreiber, T. Velkov and J. Li, *Adv. Sci.*, 2020, **7**, 2000704.
28 CLSI, *Methods for Dilution Antimicrobial Susceptibility Tests for Bacteria That Grow Aerobically. 11th ed. CLSI standard M07*, Clinical and Laboratory Standards Institute, Wayne, PA, 2018.
29 I. Wiegand, K. Hilpert and R. E. Hancock, *Nat. Protoc.*, 2008, **3**, 163–175.
30 T. Haug, A. K. Kjuul, O. B. Styrvold, E. Sandsdalen, Ø. M. Olsen and K. Stensvåg, *J. Invertebr. Pathol.*, 2002, **81**, 94–102.
31 G. V. Paesschen and D. Timmerman, *Makromol. Chem.*, 1964, **78**, 112–120.
32 M. A. Noordegraaf, G. J. Kuiper, A. T. M. Marcelis and E. J. R. Sudholter, *Macromol. Chem. Phys.*, 1997, **198**, 3681–3697.
33 N. Z. Hardin, T. Ravula, G. D. Mauro and A. Ramamoorthy, *Small*, 2019, **15**, e1804813.
34 C. Vargas, R. C. Arenas, E. Frotscher and S. Keller, *Nanoscale*, 2015, **7**, 20685–20696.
35 A. Laguerre, F. Lohr, E. Henrich, B. Hoffmann, N. Abdul-Manan, P. J. Connolly, E. Perozo, J. M. Moore, F. Bernhard and V. Dotsch, *Structure*, 2016, **24**, 1830–1841.

 This journal is © The Royal Society of Chemistry 2023

Published on 18 July 2023. Downloaded by University of Alberta on 8/1/2023 12:02:35 PM.

36 M. Azouz, M. Gonin, S. Fiedler, J. Faherty, M. Decossas, C. Cullin, S. Villette, M. Lafleur, I. D. Alves, S. Lecomte and A. Ciaccafava, *Biochim. Biophys. Acta - Biomembr.*, 2020, **1862**, 183215.
37 J. Radoicic, S. H. Park and S. J. Opella, *Biophys. J.*, 2018, **115**, 22–25.
38 A. Grethen, A. O. Oluwole, B. Danielczak, C. Vargas and S. Keller, *Sci. Rep.*, 2017, **7**, 11517.
39 S. Bhattacharjee, *J. Controlled Release*, 2016, **235**, 337–351.
40 K. Yasuhara, J. Arakida, T. Ravula, S. K. Ramadugu, B. Sahoo, J. I. Kikuchi and A. Ramamoorthy, *J. Am. Chem. Soc.*, 2017, **139**, 18657–18663.
41 T. Bengtsen, V. L. Holm, L. R. Kjolbye, S. R. Midtgaard, N. T. Johansen, G. Tesei, S. Bottaro, B. Schiott, L. Arleth and K. Lindorff-Larsen, *eLife*, 2020, **9**, e56518.
42 N. Skar-Gislinge, J. B. Jsimonsen, K. Mortensen, R. Feidenhans'l, S. G. Sligar, B. L. Møller, T. Bjørnholm and L. Arleth, *J. Am. Chem. Soc.*, 2010, **132**, 13713–13722.
43 D. Martinez, M. Decossas, J. Kowal, L. Frey, H. Stahlberg, E. J. Dufourc, R. Riek, B. Habenstein, S. Bibow and A. Loquet, *ChemPhysChem*, 2017, **18**, 2651–2657.
44 M. R. Moya-Quiles, E. Mufioz-Delgado and C. J. Vidal, *Chem. Phys. Lipids*, 1996, **79**, 21–28.
45 B. M. Stott, M. P. Vu, C. O. McLemore, M. S. Lund, E. Gibbons, T. J. Brueseke, H. A. Wilson-Ashworth and J. D. Bell, *J. Lipid Res.*, 2008, **49**, 1202–1215.
46 F. M. Harris, K. B. Best and J. D. Bell, *Biochim. Biophys. Acta, Biomembr.*, 2002, **1565**, 123–128.
47 I. G. Denisov, M. A. McLean, A. W. Shaw, Y. V. Grinkova and S. G. Sligar, *J. Phys. Chem. B*, 2005, **109**, 15580–15588.
48 M. Tanaka, A. Hosotani, Y. Tachibana, M. Nakano, K. Iwasaki, T. Kawakami and T. Mukai, *Langmuir*, 2015, **31**, 12719–12726.
49 S. Osella, N. Smisdom, M. Ameloot and S. Knippenberg, *Langmuir*, 2019, **35**, 11471–11481.
50 Q. Waheed, R. Tjornhammar and O. Edholm, *Biophys. J.*, 2012, **103**, 2125–2133.
51 X. Zhang, K. M. Barraza and J. L. Beauchamp, *Proc. Natl. Acad. Sci. U. S. A.*, 2018, **115**, 3255–3260.
52 J. T. Cheng, J. D. Hale, M. Elliott, R. E. Hancock and S. K. Straus, *Biochim. Biophys. Acta, Biomembr.*, 2011, **1808**, 622–633.
53 A. Som and G. N. Tew, *J. Phys. Chem. B*, 2008, **112**, 3495–3502.
54 S. Scheidelaar, M. C. Koorengevel, C. A. van Walree, J. J. Dominguez, J. M. Dorr and J. A. Killian, *Biophys. J.*, 2016, **111**, 1974–1986.
55 S. Chevalier, E. Bouffartigues, J. Bodilis, O. Maillot, O. Lesouhaitier, M. G. J. Feuilloley, N. Orange, A. Dufour and P. Cornelis, *FEMS Microbiol. Rev.*, 2017, **41**, 698–722.
56 P. Prasad and S. Gupta, *ACS Appl. Bio Mater.*, 2020, **3**, 8271–8285.
57 J. M. Andrews, *J. Antimicrob. Chemother.*, 2001, **48**, S5–S16.
58 J. G. Hurdle, A. J. O'Neill, I. Chopra and R. E. Lee, *Nat. Rev. Microbiol.*, 2011, **9**, 62–75.
59 K. E. Locock, T. D. Michl, J. D. Valentin, K. Vasilev, J. D. Hayball, Y. Qu, A. Traven, H. J. Griesser, L. Meagher and M. Haeussler, *Biomacromolecules*, 2013, **14**, 4021–4031.
60 S. J. Lam, E. H. H. Wong, C. Boyer and G. G. Qiao, *Prog. Polym. Sci.*, 2018, **76**, 40–64.
61 L. Liu, X. Wang, S. Zhu and L. Li, *ACS Appl. Bio Mater.*, 2021, **4**, 1211–1220.